BNL-94621-2011-JA

HOW IMPORTANT IS ORGANIC AEROSOL HYGROSCOPICITY TO AEROSOL INDIRECT FORCING?

Xiaohong Liu
Pacific Northwest National Laboratory, Richland, WA, USA

Jian Wang
Brookhaven National Laboratory, Upton, NY, USA

Submitted to Environmental Research Letters

Revised October 2010

Atmospheric Sciences Division/Environmental Sciences Dept.

Brookhaven National Laboratory

U.S. Department of Energy
Office of Science

DISCLAIMER

How Important Is Organic Aerosol Hygroscopicity to Aerosol Indirect Forcing?

Xiaohong Liu
Pacific Northwest National Laboratory, Richland, WA, USA

Jian Wang
Brookhaven National Laboratory, Upton, NY, USA

Submitted to *Environmental Research Letters*, August 2010
Revised October 2010

Corresponding author:

Xiaohong Liu
Atmospheric Science & Global Change Division
Pacific Northwest National Laboratory
3200 Q Ave., MSIN K9-24
Richland, WA 99352
U.S.A.

Tel: (509) 372-4528 (o)
Fax: (509) 375-6448
E-mail: Xiaohong.Liu@pnl.gov

Abstract

Organics are among the most abundant aerosol components in the atmosphere. However, there are still large uncertainties with emissions of primary organic aerosol (POA) and volatile organic compounds (VOCs) (precursor gases of secondary organic aerosol, SOA), formation of SOA, and chemical and physical properties (e.g., hygroscopicity) of POA and SOA. All these may have significant impacts on aerosol direct and indirect forcing estimated from global models. In this study a modal aerosol module (MAM) in the NCAR Community Atmospheric Model (CAM) is used to examine sensitivities of aerosol indirect forcing to hygroscopicity (represented by a single parameter "κ") of POA and SOA. Our model simulation indicates that in the present-day (PD) condition changing "κ" value of POA from 0 to 0.1 increases the number concentration of cloud condensational nuclei (CCN) at supersaturation S=0.1% by 40-80% over the POA source regions, while changing "κ" value of SOA by ±50% (from 0.14 to 0.07 and 0.21) changes the CCN concentration within 40%. There are disproportionally larger changes in CCN concentration in the pre-industrial (PI) condition. Due to the stronger impact of organics hygroscopicity on CCN and cloud droplet number concentration at PI condition, global annual mean anthropogenic aerosol indirect forcing (AIF) between PD and PI conditions reduces with the increase of the hygroscopicity of organics. Global annual mean AIF varies by 0.4 W m^{-2} in the sensitivity runs with the control run of -1.3 W m^{-2}, highlighting the need for improved understanding of organics hygroscopicity and its representation in global models.

1. Introduction

Atmospheric aerosols affect the global energy budget by scattering and absorbing sunlight (direct effects) and by changing the microphysics, lifetime, and coverage of clouds (indirect effects). An increase in aerosol concentration would lead to smaller cloud droplet size and higher cloud albedo, i.e., brighter clouds (Twomey, 1977). This effect, which is known as the first indirect aerosol effect, tends to cool the global climate. The smaller cloud droplet size resulting from increased aerosol concentration also inhibits precipitation, leading to an increase in cloud lifetime and coverage (second indirect aerosol effect, Albrecht, 1989). Although it is widely accepted that the indirect effects can strongly influence the global climate, and potentially mask the warming effect due to anthropogenic CO_2, the magnitudes of indirect aerosol effects are poorly understood. The Intergovernmental Panel on Climate Change (IPCC, 2007) considers the indirect effects of aerosol the most uncertain components in forcing of climate change over the industrial period.

To understand the aerosol indirect effects requires knowledge of cloud condensation nuclei (CCN) spectrum of aerosol particles, which is the number concentration of particles that can form cloud droplets as a function of water vapor supersaturation. The hygroscopicity of particles containing only soluble inorganic species typically found in atmospheric aerosols are well understood, and the CCN spectrum of the inorganic particles can be effectively predicted using Köhler theory (Köhler, 1936). However, the composition of atmospheric particles is often very complex. Compared to inorganic component usually limited to a few species, the organic component of ambient aerosols may consist of hundreds or even thousands of species,

which often contribute substantially to, or sometimes even dominate fine aerosol mass (Kanakidou et al., 2005). A number of studies have shown that organic aerosols play an important role in both the direct and indirect aerosol forcing (e.g., Lohmann et al., 2000; Chung and Seinfeld, 2002; Kanakidou et al., 2005; Goto et al., 2008), which are highly uncertain (IPCC 2007). Direct radiative forcing of anthropogenic organic aerosol was estimated to be -0.06 to -0.23 W m^{-2} as compared to -0.16 to -0.58 W m^{-2} for anthropogenic sulfate from nine global models with the same prescribed emissions (Schulz et al., 2006). At present there are large uncertainties in the emission inventories of primary organics aerosols and secondary aerosol formation in global models (Kanakidou et al., 2005; Farina et al., 2010). Furthermore, unlike typical inorganic aerosol species whose hygroscopicities are well understood, currently there are still large uncertainties in our understanding of the hygroscopicity of the organic species. Previous studies show atmospheric organics ranging from non-hygroscopic, such as primary organic aerosol emitted from fossil-fuel combustion, to highly hygroscopic biomass burning organic aerosols (Carrico et al., 2008; Petters et al., 2009). Given the computational constraints, the large number of organic species often can only be represented by no more than a few classes in global models. This presents further challenges in simulating aerosol indirect forcing (AIF). In this study, a version of NCAR Community Atmospheric Model (CAM) is used to examine the uncertainties in global simulated CCN concentration, cloud droplet number concentration (CDNC), and AIF arising from the uncertainty in our understanding of organic aerosol hygroscopicity. In the CAM, the activation of aerosol particles is represented using a parameterization (Abdul-Razzak and Ghan, 2000) based on Köhler theory, which directly takes into

consideration the effect of particle size, composition, and hygroscopicity of participating species (including organics) on particle activation. As far as we know, this is the first study examining the uncertainty in global averaged AIF due to the uncertainties in organic hygroscopicity. The implication on future study of the hygroscopicity of organic aerosol is also discussed.

2. Model

We use the NCAR Community Atmospheric Model (CAM) for all the simulations. This model version starts with CAM version 3 (Collins et al., 2006) with several important changes added. The deep convection scheme closure has been modified following Neale et al. (2008). The shallow convection scheme is based on Park and Bretherton (2009), and the moisture boundary layer scheme is based on Bretherton and Park (2009). The radiation code has been updated to the Rapid Radiative Transfer Model for GCMs (RRTMG) as described by Iacono et al. (2008). The liquid cloud macrophysics closure is described by Park et al., (2010: Revised Stratiform Macrophysics in the Community Atmosphere Model, in preparation). This CAM version is designed to simulate fully interactive aerosol direct and indirect effects. For that, a two-moment stratiform cloud microphysics is included which predicts mass and number mixing ratio of cloud water and cloud ice, and diagnoses mass and number mixing ratio of precipitation (rain and snow) (Morrison and Gettelman, 2008). The cloud ice microphysics was further modified to allow ice supersaturation and aerosol effect on ice clouds (Gettelman et al., 2010).

The new modal aerosol module (MAM) is based on Easter et al. (2004) but

includes many updates for aerosol treatment and is added with a simplified 3-mode version for long-term climate simulations (Liu et al. 2010). The benchmark version of MAM with 7 aerosol modes (MAM-7) is used here. It includes Aitken, accumulation, primary carbon, fine dust and sea salt and coarse dust and sea salt modes. The predicted internally mixed aerosol species for each log-normal mode in MAM-7 are listed in Table 1. In MAM, the interstitial aerosol particles that are suspended in air (either clear or cloudy air) and the aerosol particles in stratiform cloud droplets (referred to as cloud-borne aerosol particles) are both explicitly predicted, as in Easter et al. (2004). The cloud-borne aerosol particles are not transported, which saves computer time but have little impact on their predicted values (Ghan and Easter, 2006). Below we will provide more description on the treatment of organic aerosol and aerosol activation most relevant to this study. Further detailed description on aerosol processes and properties treated in MAM can be found in the CAM scientific document (Neale et al., 2010).

In MAM, the organic species are grouped into two classes. The first class, named as primary organic aerosol (POA), includes primary organics emitted due to both fossil fuel and bio-fuel consumption (industry, energy, transportation, agriculture waste burning, waste treatment, domestic emission and shipping) and biomass burning (forest fire and grass fire) (Lamarque et al., 2010). The second class, referred to as secondary organic aerosol (SOA), includes secondary organics formed from anthropogenic and biogenic precursors. Carbonaceous aerosols (POA and black carbon (BC)) are emitted in the primary carbon mode (see Table 1) and age to the accumulation mode through condensation of sulfuric acid gas (H_2SO_4), ammonia (NH_3), and secondary organic aerosol gas (SOA(gas)) and coagulation with Aitken and accumulation mode. The

simplest treatment of SOA, which is used in many global models, is to assume fixed mass yields for anthropogenic and biogenic volatile organic compounds (VOCs), then directly emit this mass as primary aerosol particles. MAM adds one additional step of complexity by simulating a single lumped gas-phase SOA (gas) species. Fixed mass yields with values of 5%, 5%, 15%, 4% and 25% are assumed for big alkanes, big alkenes, toluene, isoprene and monoterpenes, respectively of the five VOC categories in the MOZART-4 gas-phase chemical mechanism (Emmons et al., 2010). References for these yields can be found in Neale et al. (2010). The total yielded mass is emitted as the SOA (gas) species. MAM then calculates condensation/evaporation of the SOA (gas) to/from aerosol modes (Aitken and accumulation mode).

Organic aerosol can affect stratiform cloud microphysics through participating in activation. The hygroscopicity of each component (including POA and SOA) is prescribed in MAM, and the volume mean hygroscopicity for each aerosol mode containing different components is calculated (Ghan and Zaveri, 2007). Aerosol activation is parameterized in terms of sub-grid cloud scale vertical velocity, size distribution and volume mean hygroscopicity of all of the aerosol modes (Abdul-Razzak and Ghan, 2000). The updraft velocity is approximated by the square root of the turbulence kinetic energy, and with a minimum value of 0.2 m s^{-1}. A peak supersaturation is diagnosed in the Abdul-Razzak and Ghan (2000) parameterization which determines the critical size of aerosols in each mode activated to become cloud droplets. We note that currently the effects of organic aerosol on convective and ice cloud microphysics are not included in CAM.

The hygroscopicities of POA and SOA are parameterized using the *B* value

(Hudson and Da, 1996), which is practically equivalent to the single parameter κ proposed by Petters and Kreidenweis (2007). In this study, the single parameter κ is used, as many recent measurements of organic hygroscopicity are reported in κ. Table 2 lists the κ of secondary organics aerosols and biomass burning organic aerosol reported from previous studies, including field measurements and environmental chamber studies. While fossil fuel primary organics are generally considered as non-hygroscopic (i.e. κ=0), previous studies show that biomass burning organic aerosol and secondary organic aerosols are generally hygroscopic with κ ranged from 0.06 to 0.30. In addition, previous field studies suggest hygroscopicity of SOA increases from ~0 to 0.2 during its aging in the atmosphere (Jimenez et al., 2009). To test the effects of hygroscopicity of organic aerosol on CCN and indirect forcing, we run CAM by varying "κ" values for POA and SOA as listed in Table 3, for pairs of present-day (PD) and pre-industrial (PI) simulations. In one of the cases, κ of the POA is increased from 0 in control case to 0.1 to account for the hygroscopicity of biomass burning organics. The κ of SOA is also varied from 0.14 in the control case by ±50% to represent the range of κ of SOA reported from earlier measurements.

3. Results

The CAM model is run for 5 years with 3-month spin-up with fixed sea surface temperatures. Anthropogenic (defined here as originating from industrial, domestic and agriculture activity sectors) emissions are from the Lamarque et al. (2010) IPCC AR5 emission data set for the year 2000 (PD simulation) and year 1850 (PI simulation). The IPCC AR5 emission data set does not provide injection heights. We used the injection

heights from the AEROCOM emission protocol (Dentener et al., 2006) to distribute the IPCC AR5 emissions from energy and industrial sectors at 100-300 m above the surface, and emissions from forest fire and grass fire at 0-6 km. We used the size distributions of primary emitted particles (sulfate, POA and BC) from the AEROCOM (Dentener et al., 2006) to convert IPCC AR5 mass emission fluxes to number emission fluxes. For POA/BC, the emitted number mean radius is 0.04 μm with a standard deviation of 1.8. IPCC AR5 emission data set does not provide emissions for natural aerosols and precursor gases (e.g., volcanic sulfur, dimethylsulfide (DMS)), for which we have followed the AEROCOM protocols (Dentener et al., 2006).

Figure 1 shows annual means of column burden concentrations of POA in primary carbon mode and POA aged to the accumulation mode, and SOA from the PD and PI control run. Clearly POA from primary emissions (e.g., fossil fuel, bio-fuel, and biomass burning) is aged to the accumulation mode quickly, e.g., at PD in the industrial regions where sulfate concentrations are high. This result is in general agreement with observations that carbonaceous aerosol particles are internally mixed with sulfate and other components except near the source regions (e.g., Posfai et al., 2003; Clarke et al., 2004; Moffet and Prather, 2009; Wang et al., 2010). SOA column concentrations have the spatial distributions similar to aged POA, and both have high concentrations in the industrial regions and in the biomass burning regions (central Africa and South America), although their seasonal variations are different (results not shown). The global spatial distributions of POA (in primary and accumulation modes) and SOA column concentrations are similar between PD and PI. However, there are several noticeable differences: aged POA concentration in the accumulation mode at PD in South and East

Asia, Indonesia and in central Africa and South America is much higher than that at PI due to emission differences, while POA concentration in Eastern U.S. is higher at PI due to more emissions from forest and grass fire and domestic heating there at PI (Lamarque et al., 2010).

The global budgets for organic aerosol (POA in primary and accumulation mode, and SOA) are given in Table 4. POA in the primary mode ages to the accumulation mode with a lifetime of 1.2-1.5 days. There is a longer lifetime for POA in the primary mode at PI than that at PD due to significantly less sulfate available for aging at PI (see Figure 2 below). Global burden of aged POA in the accumulation mode is 4-6 times higher than that in the primary mode. Fossil and bio-fuel POA emissions at PI is 36% of that at PD, however, that from biomass burning emissions at PI is 78% of that at PD. Total POA at PI is 63% of that at PD mainly due to the lower fossil fuel and bio-fuel POA emission sources at PI. SOA (g) formation is dominated from the oxidation of biogenic VOCs (isoprene and monoterpenes) in this study. Therefore we see only a slightly reduction of SOA burden (by 10%) at PI compared to PD. The global SOA production (68.6 Tg yr^{-1} at PD) in this study is higher than 11.2 Tg yr^{-1} from the earlier studies by Chung and Seinfeld (2002), 19.1 Tg yr^{-1} by Dentener et al. (2006), 10-60 Tg yr^{-1} by Kanakidou et al. (2005), and within the range of 28.9 to 75.1 Tg yr^{-1} from a more recent study by Farina et al. (2010). The SOA burden of 1.26 Tg at PD in this study is higher than 0.19 Tg from Chung and Seinfeld (2002), but within the range of 0.54-2.4 Tg from Farina et al. (2010).

Figure 2 shows annual means of column burden concentrations of sulfate from the PD and PI control run. Sulfate column concentrations have maximum values in the industrial regions (Asia, North America and Europe) at PD, and are significantly lower at

PI. At PD, sulfate column concentrations are slightly higher than those of aged POA and SOA in the industrial regions, whereas at PI, sulfate column concentrations are much lower (e.g., in Asia and North America). The global annual burden of sulfate is 0.61 Tg S at PD (within the range of 0.53-1.07 Tg S from literature collected in Liu et al., 2005) and 0.21 Tg S at PI.

Figure 3 shows percentage changes of cloud condensational nuclei (CCN) concentration at supersaturation of 0.1% at 859 hPa between the sensitivity simulations listed in Table 3 and the control (CTL) simulation at PD and at PI. Here CCN concentration diagnosed at a given supersaturation (0.1%) is used to show the impact of aerosols on cloud droplet number concentration, as the spatial distribution of changes in model predicted cloud droplet number concentration between different simulations is quite noisy due to cloud dynamical and thermodynamical feedbacks. CCN concentration at a given supersaturation is determined by a parameterization based on Köhler theory (Ghan and Zaveri, 2007). The parameterization takes into consideration both the aerosol size distribution (represented by each mode) and volume weighted κ value from aerosol components (including organics) in each mode. For a given supersaturation and a fixed size distribution, an increase in κ value leads to lower critical dry size for activation, and higher CCN concentration as predicted from Köhler theory. From Figure 3 at PD, an increase in κ value for POA from 0 to 0.1 increases CCN concentrations at 859 hPa by 20-80% over the POA source regions (see Figure 1). There are also some reductions by 10-20% in the Arctic in the downwind of Siberia and Northern Canada due to more scavenging of POA in primary carbon mode when activated into cloud droplets at a higher κ value. A reduction of κ value for SOA from 0.14 to 0.07 at PD leads to

reductions of CCN concentrations almost everywhere over the continents. The rainforest source regions (e.g, central Africa and South America) have reductions of 20-40%, as well as in the boreal and Arctic regions. CCN number reductions in the industrial regions are small (within 10%) because there is sufficient sulfate there to compensate aerosol hygroscopicity reduction due to SOA. An increase of κ value for SOA from 0.14 to 0.21 at PD has the similar impact on CCN concentrations as increasing κ value for POA although the magnitude is smaller (within 40% increase).

Figure 3 also shows the changes of CCN concentration at PI. In general same changes in κ value have much larger effects on CCN concentration at PI compared to those at PD. An increase in POA κ value increases CCN concentration significantly in the industrial source regions (North America, Asia, and Europe) at PI, which is, however, much less pronounced at PD. As indicated in Figure 2, POA is aged to the accumulation mode and internally mixed with sulfate and other components quickly, especially in the industrial regions (e.g., Asia) and at PD when sulfate concentrations are higher than those at PI. As a result, the variation in CCN concentration resulted from varying POA κ is generally small in the industrial regions at PD. This is in agreement with earlier studies that show for internally mixed particles, their hygroscopicity is dominated by inorganics such as sulfate and ammonium, and the influence of organic hygroscopicity on calculated CCN concentration is often minor there (Chang et al., 2007; Prenni et al., 2007; Wang et al., 2008). In contrast, at PI when sulfate loading is substantially less, organics represent a larger fraction of particle volume. As a result, an increase in κ value of POA leads to relatively larger increase in calculated CCN concentration. This disproportional change in CCN concentration can also be found with a reduction or increase in SOA κ value.

Table 5 gives the global annual mean vertically-integrated (column) CCN concentration at supersaturation of 0.1% and column cloud droplet number concentration (CDNUMC) for all four runs listed in Table 3 at PD and PI. Clearly there are larger changes in both CCN and CDNUMC concentrations at PI compared to PD as κ values vary. We note that global mean CCN column concentration at supersaturation of 0.1% is substantially higher than CDNUMC. This is because CCN concentration at supersaturation of 0.1% is calculated for the three-dimensional aerosol fields predicted in the model, whereas model predicted cloud droplet number concentration is limited to the cloudy regions where cloud droplets exist.

Figure 4 shows annual zonal mean changes of CDNUMC, shortwave cloud forcing (SWCF), liquid water path (LWP) and low-level cloud cover (CLDLOW) between PD and PI for the four simulations listed in Table 3. We note that cloud response to anthropogenic aerosol perturbations may be noisy especially in the southern hemisphere (SH) due to natural variability and feedbacks of cloud dynamics and thermodynamics. However, we can clearly see that the SWCF increases (more negative) by as much as 4 W m^{-2} in the northern hemisphere (NH) mid-latitudes due to more numerous and smaller cloud droplets in PD compared to PI. An increase of LWP by 10 g m^{-2} is found in the NH mid-latitudes due to the second aerosol indirect effect to slow down the autoconversion of cloud water to rain. In addition, CLDLOW increases by 2-3% in the NH high latitudes due to Arctic amplification from snow-ice feedbacks. Comparing with the control run, a higher κ value of POA (POA-hiK run) reduces the difference of CDNUMC between PD and PI (e.g., in 20-60 °N by 20-30%) due to more CCN and cloud droplet number increase at PI. Correspondingly, SWCF and LWP

changes between PD and PI are reduced. A lower κ value of SOA (SOA-loK run) enhances the difference in CDNUMC between PD and PI (e.g., in 20-60 °N and in 20-30 °S) due to more CCN and cloud droplet number reduction at PI, and thus changes in SWCF and LWP between PD and PI are increased (e.g., in 20-60 °N and in the tropics). Similarly, a higher κ value of SOA (SOA-hiK run) reduces the differences of CDNUMC, SWCF and LWP between PD and PI. Changes in CLDLOW between PD and PI are not much different between different runs except in the Arctic regions for SOA-hiK run. However, in the high latitudes where surface areas are relatively small the change signals may be just due to natural noise.

The global, NH and SH annual mean changes between PD and PI of SWCF, LWP, CLDLOW and CDNUMC for different runs are listed in Table 6. AIF is defined here as SWCF change between PD and PI as LWCF change is much smaller (0.1 W m^{-2}). We can see that AIF has the largest difference between POA-hiK and SOA-loK runs (by 0.4 W m^{-2} on the global mean) along with largest change in ΔLWP between these two runs (by 1 g m^{-2} on the global mean), in consistent with the smallest increase in POA-hiK (4.6×10^{9} m^{-2} on the global mean) and the largest increase of CDNUMC between PD and PI in SOA-loK (5.2×10^{9} m^{-2} on the global mean). Changes between PD and PI (ΔSWCF, ΔLWP, ΔCLDLOW and ΔCDNUMC) for all four runs occur mainly in the NH due to more anthropogenic emissions. Differences of ΔSWCF, ΔLWP and ΔCDNUMC between different runs with varying κ value are also larger in the NH than those in the SH.

4. Discussion

There are large uncertainties in both the sources and the properties of organic aerosol. In this study we focus on the sensitivity of modeled AIF to the hygroscopicity of organic aerosol, which influences the ability of particles to activate into cloud droplets. The simulation results show that the uncertainty in organics aerosol hygroscopicity, based on current understanding and our model formulation, may lead to an uncertainty of about 0.4 W m^{-2} (-1.1 to -1.5 W m^{-2}) in AIF, which represents 1/3 of AIF simulated in the control case (-1.3 W m^{-2}). This uncertainty is comparable or even larger than those due to autoconversion parameterization and tuning parameters related to entrainment, drizzle and snow formation (Liu et al., 2008; Lohmann and Ferrachat, 2010).

As expected, AIF is most significant in the NH, where anthropogenic influence is the strongest. It is worth noting whereas a variation in organic hygroscopicity may lead to substantial changes in CCN concentration and CDNC in pristine environments (e.g. tropical forest), such changes have no impact on AIF there in the absence of anthropogenic aerosols, as AIF represents the difference between PD and PI. However, our results also highlight the important impact on AIF from organic aerosol, especially in the polluted NH mid-latitudes. Whereas an increase of POA κ from 0 (control run) to 0.1 (POA-hiK run) leads to expected increases in CCN concentration at PD, the increase of CDNC from PI to PD is reduced, and the AIF decreases from -1.3 to -1.1 W m^{-2} at the higher κ value of POA. This is due to disproportional impacts of POA κ on CCN concentration at PD and PI in areas with substantial anthropogenic influence at PD (e.g., NH mid-latitudes). Such feature is highlighted in Figure 3, which shows larger increases in CCN concentration due to the increase of POA κ at PI compared to those at PD, especially in the industrial regions. This disproportional change in CCN concentration

reduces the magnitude of the perturbation due to anthropogenic influences as we can see that the CDNUMC change from PI to PD in Figure 4 and Table 6 is reduced. Similarly, a decrease in κ value of SOA (SOA-loK run) leads to more pronounced decrease in CCN concentration at PI compared to PD, and therefore increases CDNUMC and LWP differences between PD and PI and thus AIF. Given the large contribution of biogenic SOA and biomass burning POA to the budget of organic aerosol, further constraint of their hygroscopicity in global models will help to reduce the uncertainty in simulated AIF.

An implicit assumption in the simulations is that for both organics classes, their hygroscopicities do not change from PI to PD. Anthropogenic emissions can strongly influence ozone and nitrogen oxide (NO_x) concentrations, which have been shown to impact the formation of secondary organic aerosols (Kanakidou et al., 2005, Presto et al., 2005; Dommen et al., 2006; Kroll et al., 2006; Ng et al., 2007; Carlton et al., 2009). Studies also suggest the VOC to NO_x ratio may influence the composition of SOA formed from biogenic VOC and therefore potentially its κ value. A recent study finds little variation in κ of SOA formed from isoprene photooxidation at different VOC to NO_x ratios (King et al., 2010). However, there have been essentially no studies on the impact of NO_x on κ of SOA formed from other biogenic precursors. While SOA κ may have relatively small impact on calculated CCN concentration for PD due to the internally mixing with high-hygroscopic inorganic species, this change of SOA κ from PI to PD as a result of anthropogenic influence may lead to additional uncertainty in simulated AIF.

The biomass burning organics and biogenic secondary organics dominate the budgets of POA and SOA, especially for PI. Currently, experimentally determined κ of SOA and biomass burning POA shows a range of 0.06 to ~0.3. Given the importance of understanding the CCN concentration at PI, κ of SOA and biomass burning POA need to be better understood and represented in models to reduce the uncertainties in AIF. As fossil fuel POA and biomass burning POA have quite different hygroscopicities, separating the two types of POA in future model development would improve the simulation of AIF. Furthermore, aging processes in the atmosphere can also lead to the increase of hygroscopicity of POA and SOA. Field studies suggest κ of SOA increases from 0 to ~0.2 during aging in the atmosphere (Jimenez et al., 2009), a range that is even greater than that simulated in the current study. The representation of this change of κ due to atmospheric aging is also an important step for improving the simulation of AIF. Besides organics hygroscopicity, large uncertainties also exist on the SOA formation simulated in global models. The impact of organics formation on AIF will be examined in future studies.

Acknowledgments:

X. Liu was funded by the US Department of Energy, Office of Science, Atmospheric System Research (ASR) program and Scientific Discovery through Advanced Computing (SciDAC) program. J. Wang is funded by the US Department of Energy, Office of Science, ASR program. The Pacific Northwest National Laboratory is operated for DOE by Battelle Memorial Institute under contract DE-AC06-76RLO 1830. The Brookhaven National Laboratory is operated for DOE by Brookhaven Science Associates, LLC under

Contract DE-AC02-98CH10886.

References

Abdul-Razzak, H. and S. J. Ghan (2000), A parameterization of aerosol activation 2. Multiple aerosol types, *J. Geophys. Res.*, 105(D5): 6837-6844.

Albrecht, B. A. (1989), Aerosols, cloud microphysics, and fractional cloudiness, *Science*, *245*, 1227-1230.

Asa-Awuku, A., A. P. Sullivan, C. J. Hennigan, R. J. Weber, and A. Nenes (2008), Investigation of molar volume and surfactant characteristics of water-soluble organic compounds in biomass burning aerosol, *Atmospheric Chemistry and Physics*, *8*, 799-812.

Bretherton, C. S., and S. Park (2009), A new moist turbulence parameterization in the Community Atmosphere Model, *J. Clim.*, 22, 3422–3448.

Carrico, C. M., M. D. Petters, S. M. Kreidenweis, J. L. Collett, G. Engling, and W. C. Malm (2008), Aerosol hygroscopicity and cloud droplet activation of extracts of filters from biomass burning experiments, *J. Geophys. Res.*, *113*, D08206.

Carlton, A. G., C. Wiedinmyer, and J. H. Kroll (2009), A review of Secondary Organic Aerosol (SOA) formation from isoprene, *Atmospheric Chemistry and Physics*, *9*, 4987-5005.

Chang, R. Y. W., P. S. K. Liu, W. R. Leaitch, and J. P. D. Abbatt (2007), Comparison between measured and predicted CCN concentrations at Egbert, Ontario: Focus on the organic aerosol fraction at a semi-rural site, *Atmos. Environ.*, *41*, 8172-8182.

Chung, S. H., and J. H. Seinfeld (2002), Global distribution and climate forcing of carbonaceous aerosols, *J. Geophys. Res.*, *107*, D19, 4407, doi:10.1029/2001JD001397.

Clarke, A. D., Y. Shinozuka, V. N. Kapustin, S. Howell, B. Huebert, S. Doherty, T. Anderson, D. Covert, J. Anderson, X. Hua, K. G. Moore, C. McNaughton, G. Carmichael, and R. Weber (2004), Size distributions and mixtures of dust and black carbon aerosol in Asian outflow: Physiochemistry and optical properties, *J. Geophys. Res.*,, *109*, D15S09.

Collins, W. D., et al. (2006), The formulation and atmospheric simulation of the Community Atmosphere Model: CAM3, *J. Clim.*, 19 (11), 2122–2161.

Dentener, F., et al. (2006) Emissions of primary aerosol and precursor gases in the years 2000 and 1750 prescribed data-sets for AeroCom, *Atmos. Chem. Phys.*, *6*, 4321-4344.

Dommen, J., A. Metzger, J. Duplissy, M. Kalberer, M. R. Alfarra, A. Gascho, E. Weingartner, A. S. H. Prevot, B. Verheggen, and U. Baltensperger (2006), Laboratory observation of oligomers in the aerosol from isoprene/NOx photooxidation, *Geophys. Res. Lett.*, *33*, L13805.

Duplissy, J., M. Gysel, M. R. Alfarra, J. Dommen, A. Metzger, A. S. H. Prevot, E. Weingartner, A. Laaksonen, T. Raatikainen, N. Good, S. F. Turner, G. McFiggans, and U. Baltensperger (2008), Cloud forming potential of secondary organic aerosol under near atmospheric conditions, *Geophys. Res. Lett.*, *35*, L03818.

Easter, R. C., et al. (2004) MIRAGE: Model description and evaluation of aerosols and trace gases, *J. Geophys. Res.*, *109*(D20): D20210,10.1029/2004jd004571.

Emmons, L. K., et al. (2010) Description and evaluation of the Model for Ozone and Related chemical Tracers, version 4 (MOZART-4), *Geosci. Model Dev.*, 3: 43-67 10.5194/gmd-3-43-2010.

Engelhart, G. J., A. Asa-Awuku, A. Nenes, and S. N. Pandis (2008), CCN activity and droplet growth kinetics of fresh and aged monoterpene secondary organic aerosol, *Atmos. Chem. Phys.*, *8*, 3937-3949.

Farina, S. C., P. J. Adams, S. N. Pandis (2010), Modeling global secondary organic aerosol formation and processing with the volatility basis set: Implications for anthropogenic secondary organic aerosol, *J. Geophys. Res.*, *115*, D09202, doi:10.1029/2009JD013046.

Gettelman, A., X. Liu, S. J. Ghan, H. Morrison, S. Park, and A. J. Conley (2010), Global simulations of ice nucleation and ice supersaturation with an improved cloud scheme in the Community Atmospheric Model, *J. Geophys. Res.*, *115*, D18216, doi:10.1029/2009JD013797.

Ghan, S. J., and R. C. Easter (2006), Impact of cloud-borne aerosol representation on aerosol direct and indirect effects, *Atmos. Chem. Phys.*, *6*, 4163–4174.

Ghan, S. J., and R. A. Zaveri (2007), Parameterization of optical properties for hydrated internally mixed aerosol, *J. Geophys. Res.*, *112*, D10201, doi:10.1029/2006JD007927.

Goto, D, T. Takemura, T. Nakajima (2008), Importance of global aerosol modeling including secondary organic aerosol formed from monoterpene, *J. Geophys. Res.*, *113*, D07205, Doi: 10.1029/2007JD009019.

Gunthe, S. S., S. M. King, D. Rose, Q. Chen, P. Roldin, D. K. Farmer, J. L. Jimenez, P. Artaxo, M. O. Andreae, S. T. Martin, and U. Pöschl (2009), Cloud condensation nuclei in pristine tropical rainforest air of Amazonia: size-resolved measurements and modeling of atmospheric aerosol composition and CCN activity, *Atmos. Chem. Phys. Discuss.*, *9*, 3811-3870.

Hudson, J. G., and X. Y. Da (1996), Volatility and size of cloud condensation nuclei, *J. Geophys. Res.*, *101*, 4435-4442.

Iacono, M. J., J. Delamere, E. Mlawer, M. Shephard, S. Clough, and W. Collins (2008), Radiative forcing by long-lived greenhouse gases: Calculations with the AER radiative transfer models, *J. Geophys. Res.*, *113* (D13103), doi:10.1029/2008JD009944.

Intergovernmental panel on Climate Change (IPCC): Climate change 2007: The physical science basis, Cambridge University Press, New York, 2007.

Jimenez, J. L., M. R. Canagaratna, N. M. Donahue, et al. (2009), Evolution of Organic Aerosols in the Atmosphere, *Science*, *326*, 1525-1529.

Juranyi, Z., M. Gysel, J. Duplissy, E. Weingartner, T. Tritscher, J. Dommen, S. Henning, M. Ziese, A. Kiselev, F. Stratmann, I. George, and U. Baltensperger (2009), Influence of gas-to-particle partitioning on the hygroscopic and droplet activation behaviour of alpha-pinene secondary organic aerosol, *Physical Chemistry Chemical Physics*, *11*, 8091-8097.

Kanakidou, M., et al. (2005), Organic aerosol and global climate modelling: a review, *Atmos. Chem. Phys.*, *5*, 1053-1123.

King, S. M., T. Rosenoern, J. E. Shilling, Q. Chen, and S. T. Martin (2007), Cloud condensation nucleus activity of secondary organic aerosol particles mixed with sulfate, *Geophys. Res. Lett.*, *34*, L24806.

King, S. M., T. Rosenoern, J. E. Shilling, Q. Chen, and S. T. Martin (2009), Increased cloud activation potential of secondary organic aerosol for atmospheric mass loadings, *Atmos. Chem. Phys.*, *9*, 2959-2971.

King, S. M., T. Rosenoern, J. E. Shilling, Q. Chen, Z. Wang, G. Biskos, K. A. McKinney, U. Poschl, and S. T. Martin (2010), Cloud droplet activation of mixed organic-sulfate particles produced by the photooxidation of isoprene, *Atmospheric Chemistry and Physics*, *10*, 3953-3964.

Köhler, H. (1936), The nucleus in and the growth of hygroscopic droplets, *Trans. Farad. Soc.*, *32*, 1152-1161.

Kroll, J. H., N. L. Ng, S. M. Murphy, R. C. Flagan, and J. H. Seinfeld (2006), Secondary organic aerosol formation from isoprene photooxidation, *Environmental Science & Technology*, *40*, 1869-1877.

Lamarque, J. F., et al. (2010) Historical (1850–2000) gridded anthropogenic and biomass burning emissions of reactive gases and aerosols: methodology and application, *Atmospheric Chemistry and Physics*, *10*, 7017–7039.

Liu, X., et al. (2008), Eos Trans AGU 89(53, Fall Meet Suppl):(abstr A32A-03).

Liu, X., R. C. Easter, S. J. Ghan, R. Zaveri, P. Rasch, X. Shi, J.-F. Lamarque, A. Gettelman, H. Morrison, F. Vitt, A. Conley, S. Park, R. Neale, C. Hannay, A. Ekman, P. Hess, N. Mahowald, W. Collins, M. Iacon, C. Bretherton, and M. Flanner (2010), Toward a Minimal Representation of Aerosol Direct and Indirect Effects, *Journal of Climate*, to be submitted.

Liu, X., J. E. Penner, and M. Herzog (2005), Global simulation of aerosol dynamics: Model description, evaluation, and interactions between sulfate and nonsulfate aerosols, *Journal of Geophysical Research*, *110*, No. D18, D18206, doi:10.1029/2004JD005674.

Lohmann, U., J. Feichter, J. Penner, and R. Leaitch (2000), Indirect effect of sulfate and carbonaceous aerosols: A mechanistic treatment, *J. Geophys. Res.*, *105*, 12193-12206.

Lohmann, U. and J. Feichter (2005), Global indirect aerosol effects: a review, *Atmospheric Chemistry and Physics*, 5: 715-737.

Lohmann, U. and Ferrachat, S. (2010), Impact of parametric uncertainties on the present-day climate and on the anthropogenic aerosol effect, *Atmos. Chem. Phys. Discuss.*, *10*, 19195-19217, doi:10.5194/acpd-10-19195-2010.

Moffet, R. C., and K. A. Prather (2009), In-situ measurements of the mixing state and optical properties of soot with implications for radiative forcing estimates, *Proc Natl Acad Sci USA*, *106*, 11872-11877.

Morrison, H. and A. Gettelman (2008), A new two-moment bulk stratiform cloud microphysics scheme in the community atmosphere model, version 3 (CAM3). Part I: Description and numerical tests, *Journal of Climate*, 21(15): 3642-3659.

Neale, R. B., J. H. Richter, and M. Jochum (2008), The Impact of Convection on ENSO: From a Delayed Oscillator to a Series of Events, *J. Clim.*, 21, 5904–+, doi: 10.1175/2008JCLI2244.1.

Neale, R., B. et al. (2010), Description of the NCAR Community Atmosphere Model (CAM 5.0), NCAR Technical Note, June 2010. http://www.cesm.ucar.edu/models/cesm1.0/cam/docs/description/cam5_desc.pdf

Ng, N. L., P. S. Chhabra, A. W. H. Chan, J. D. Surratt, J. H. Kroll, A. J. Kwan, D. C. McCabe, P. O. Wennberg, A. Sorooshian, S. M. Murphy, N. F. Dalleska, R. C. Flagan, and J. H. Seinfeld (2007), Effect of NOx level on secondary organic

aerosol (SOA) formation from the photooxidation of terpenes, *Atmospheric Chemistry and Physics*, *7*, 5159-5174.

Park, S., and C. S. Bretherton (2009), The University of Washington shallow convection and moist turbulence schemes and their impact on climate simulations with the Community Atmosphere Model, *J. Clim.*, 22, 3449–3469.

Petters, M. D., and S. M. Kreidenweis (2007), A single parameter representation of hygroscopic growth and cloud condensation nucleus activity, *Atmos. Chem. and Phys.*, *7*, 1961-1971.

Petters, M. D., C. M. Carrico, S. M. Kreidenweis, A. J. Prenni, P. J. DeMott, J. L. Collett, and H. Moosmuller (2009), Cloud condensation nucleation activity of biomass burning aerosol, *J. Geophys. Res.*, *114*, D22205.

Posfai, M., R. Simonics, J. Li, P. V. Hobbs, and P. R. Buseck (2003), Individual aerosol particles from biomass burning in southern Africa: 1. Compositions and size distributions of carbonaceous particles, *J. Geophys. Res.*, *108*, Article Number: 8483.

Prenni, A. J., M. D. Petters, S. M. Kreidenweis, P. J. DeMott, and P. J. Ziemann (2007), Cloud droplet activation of secondary organic aerosol, *J. Geophys. Res.*, *112*, D10223.

Presto, A. A., K. E. H. Hartz, and N. M. Donahue (2005), Secondary organic aerosol production from terpene ozonolysis. 2. Effect of NOx concentration, *Environmental Science & Technology*, *39*, 7046-7054.

Schulz, M., C. Textor, S. Kinne, Y. Balkanski, S. Bauer, T. Berntse, T. Berglen, O. Boucher, F. Dentener, S. Guibert, I.S.A. Isaksen, T. Iversen, D. Koch, A. Kirkevag, X. Liu, V. Montanaro, G. Myhre, J. Penner, G. Pitari, S. Reddy, O. Seland, P. Stier, and T. Takemura (2006), Radiative forcing by aerosols as derived from the AeroCom present-day and pre-industrial simulations, *Atmospheric Chemistry and Physics*, *6*, 5225-5246.

Twomey, S. (1977), Influence of Pollution on Shortwave Albedo of Clouds, *J. Atmos. Sci.*, *34*, 1149-1152.

Wang, J., Y. N. Lee, P. H. Daum, J. Jayne, and M. L. Alexander (2008), Effects of aerosol organics on cloud condensation nucleus (CCN) concentration and first indirect aerosol effect, *Atmos. Chem. Phys.*, *8*, 6325-6339.

Wang, J., Cubison, M. J., Aiken, A. C., Jimenez, J. L., and Collins, D. R. (2010), The importance of aerosol mixing state and size-resolved composition on CCN concentration and the variation of the importance with atmospheric aging of aerosols. *Atmos. Chem. Phys.*, *10*, 7267-7283.

Table 1. Predicted Species for Interstitial and Cloud-Borne Component of Each Aerosol Mode in MAM-7[a]

Aitken Mode	Accumulation Mode	Fine Soil Dust	Fine Sea Salt
number mixing ratio sulfate mmr ammonium mmr sea salt mmr secondary organic mmr	number mixing ratio sulfate mmr ammonium mmr sea salt mmr secondary organic mmr aged primary organic mmr aged BC mmr	number mixing ratio soil dust mmr sulfate mmr ammonium mmr	number mixing ratio sea salt mmr sulfate mmr ammonium mmr
	Primary Carbon Mode	Coarse Soil Dust	Coarse Sea salt
	number mixing ratio primary organic mmr BC mmr	number mixing ratio soil dust mmr sulfate mmr ammonium mmr	number mixing ratio sea salt mmr sulfate mmr ammonium mmr

[a] mmr: mass mixing ratio

Table 2. Organics Hygroscopicity from Previous Measurements

Organics Class	Range of κ	References
Biogenic SOA	0.06-0.23	Prenni et al., 2007; King et al., 2007, Duplissy et al., 2008; Engelhart et al., 2008; Gunthe et al., 2009; Juranyi et al., 2009; King et al., 2009; King et al., 2010.
Anthropogenic SOA	0.06-0.14	Prenni et al., 2007
Biomass burning organic aerosol	0.06-0.30	Vestin et al., 2007; Asa-Awuku et al., 2008; Carrico et al., 2008; Guthe et al., 2009; Petters et al., 2009

Table 3. Simulations Performed in This Study

Case Name	Description
CTL	Standard CAM, κ = 0.0 (POA), κ=0.14 (SOA)
POA-hiK	κ = 0.1 (POA), κ=0.14 (SOA)
SOA-loK	κ = 0.0 (POA), κ=0.07 (SOA)
SOA-hiK	κ = 0.0 (POA), κ=0.21 (SOA)

Table 4. Global Budgets for Organic Aerosol from the Control (CTL) Run at PD and PI

	PD	PI
POA (primary mode)		
Sources		
Fossil and bio-fuel emission	16.8	6.0
Biomass burning emission	32.5	25.2
Sinks		
Dry deposition	2.9	2.2
Wet deposition	0.005	0.003
Aged to accumulation mode	46.4	29.0
Burden	0.16	0.13
Lifetime	1.2	1.5
POA (accumulation mode)		
Sources		
Aged from primary mode	46.4	29.0
Sinks		
Dry deposition	7.2	4.8
Wet deposition	39.3	24.3
Burden	0.95	0.56
Lifetime	7.5	7.0
SOA		
Sources		
Condensation of SOA (g)	68.6	61.5
Sinks		
Dry deposition	9.8	8.1
Wet deposition	58.7	53.3
Burden	1.26	1.13
Lifetime	6.7	6.8

Units are sources and sinks, Tg yr^{-1}; burden, Tg; lifetime, days.

Table 5. Global Annual Mean Vertically-Integrated (Column) Cloud Condensational Nuclei (CCN) Concentration ($\times 10^{10}$ m^{-2}) at Supersaturation of 0.1% and Cloud Droplet Number Concentration (CDNUMC, $\times 10^{9}$ m^{-2}) for All Four Runs at PD and PI

Case Name	CTL	POA-hiK	SOA-loK	SOA-hiK
		Column CCN[a]		
PD	25.6	27.6 (+7.8%)	23.7 (-7.4%)	27.3 (+6.6%)
PI	14.9	16.7 (+12.1%)	12.9 (-13.4%)	16.6 (+11.4%)
		CDNUMC[a]		
PD	14.8	15.0 (+1.3%)	14.3 (-3.4%)	15.1 (+2.1%)
PI	9.9	10.4 (+5.1%)	9.1 (-8.1%)	10.3 (+4.0%)

[a] The values in the parenthesis are for the percentage changes of column CCN concentration and CDNUMC between the sensitivity runs (POA-hiK, SOA-loK, and SOA-hiK) and the control run (CTL) for both PD and PI.

Table 6. Global, Northern hemisphere (NH) and Southern Hemisphere (SH) Annual Mean Changes (Δ) of Shortwave Cloud Forcing (SWCF, W m^{-2}), Liquid Water Path (LWP, g m^{-2}), Low-Level Cloud Cover (CLDLOW, %), and Column Droplet Number Concentration (CDNUMC, $\times 10^9$ m^{-2}) between PD and PI (PD-PI) for All Runs

Case Name		CTL[a]	POA-hiK	SOA-loK	SOA-hiK
ΔSWCF	Global	-1.3	-1.1	-1.5	-1.2
	NH	-2.2	-1.9	-2.5	-2.0
	SH	-0.3	-0.3	-0.4	-0.4
ΔLWP	Global	3.9	3.6	4.6	3.8
	NH	6.3	5.7	7.2	6.0
	SH	1.5	1.5	2.0	1.6
ΔCLDLOW	Global	0.3	0.2	0.3	0.3
	NH	0.6	0.5	0.7	0.6
	SH	0.0	-0.1	-0.1	0.0
ΔCDNUMC	Global	4.9	4.6	5.2	4.8
	NH	8.0	7.4	8.3	7.7
	SH	1.8	1.8	2.1	1.9

[a] Global annual mean SWCF, LWP, CLDLOW, and CDNUMC of control run at PD are -47.1 W m^{-2}, 45.6 g m^{-2}, 37.1 %, and 14.8×10^9 m^{-2}, respectively.

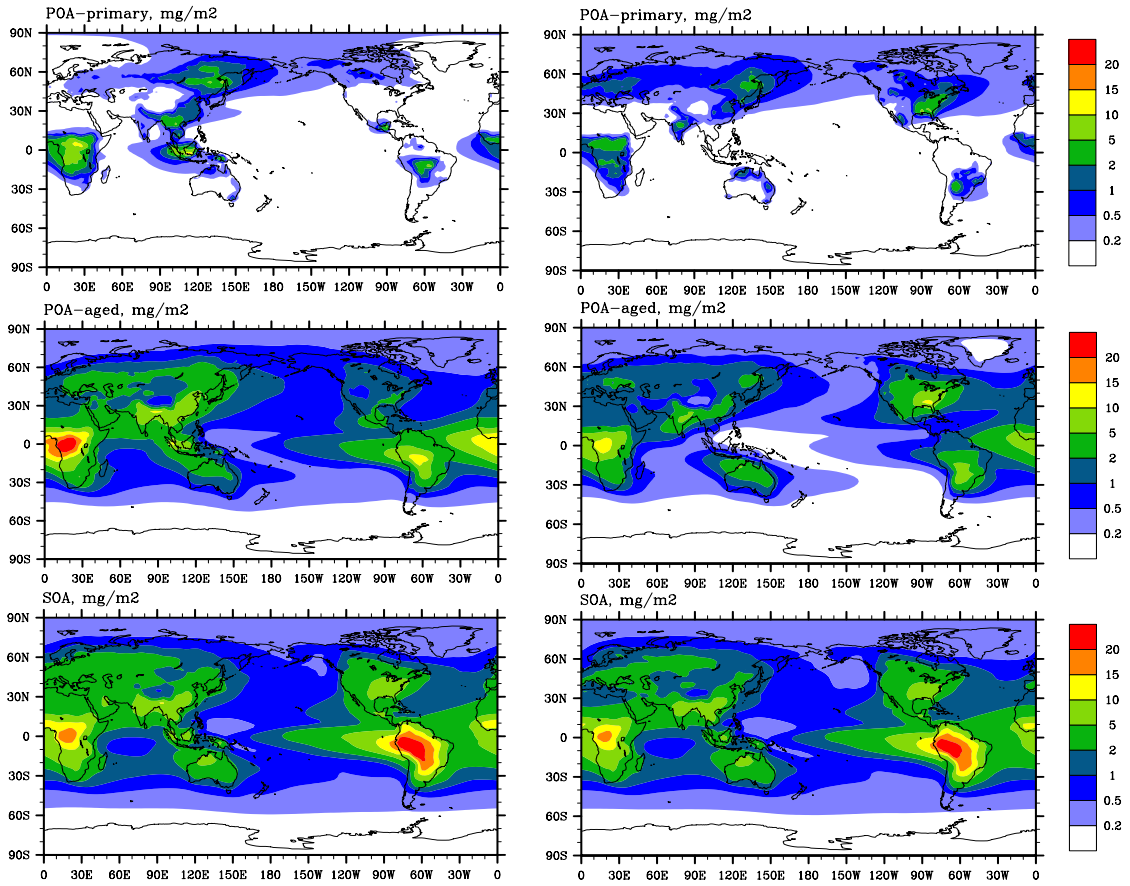

Figure 1. Annual means of column burden concentrations (mg m^{-2}) of POA in primary carbon mode (upper panel) and aged POM in the accumulation mode (middle panel), and SOA (lower panel) in the CTL run at PD (left) and at PI (right).

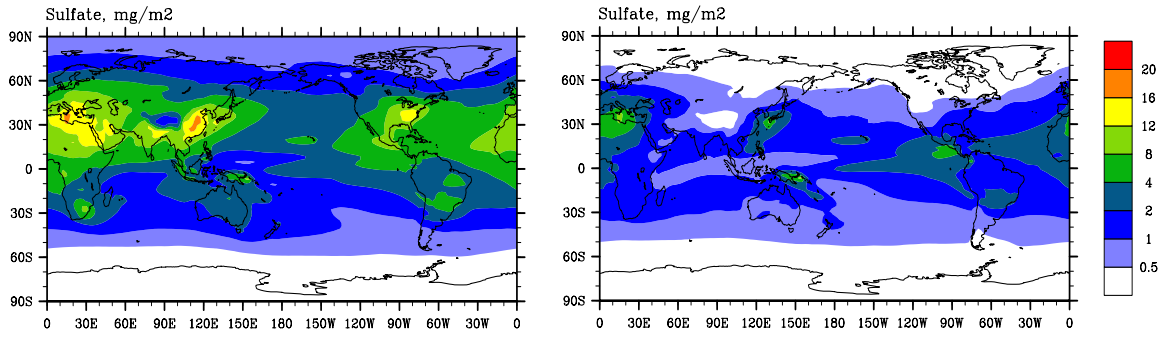

Figure 2. Annual means of column burden concentration (mg m^{-2}) of sulfate in the CTL run at PD (left) and at PI (right).

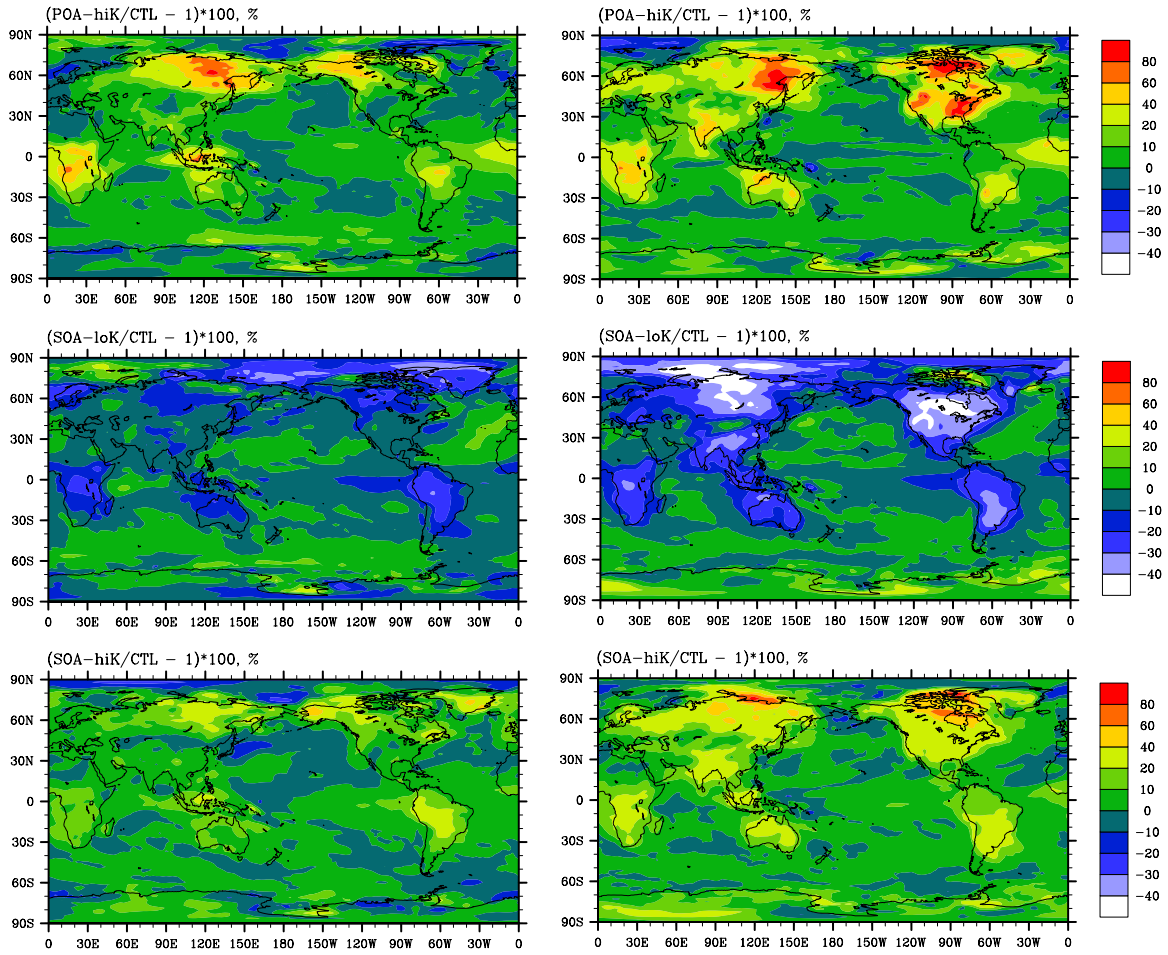

Figure 3. Percentage changes of cloud condensational nuclei (CCN) concentration at supersaturation of 0.1% at 859 hPa between the sensitivity simulations (POA-hiK, SOA-loK, and SOA-hiK) and the control simulation (CTL) at PD (left) and at PI (right).

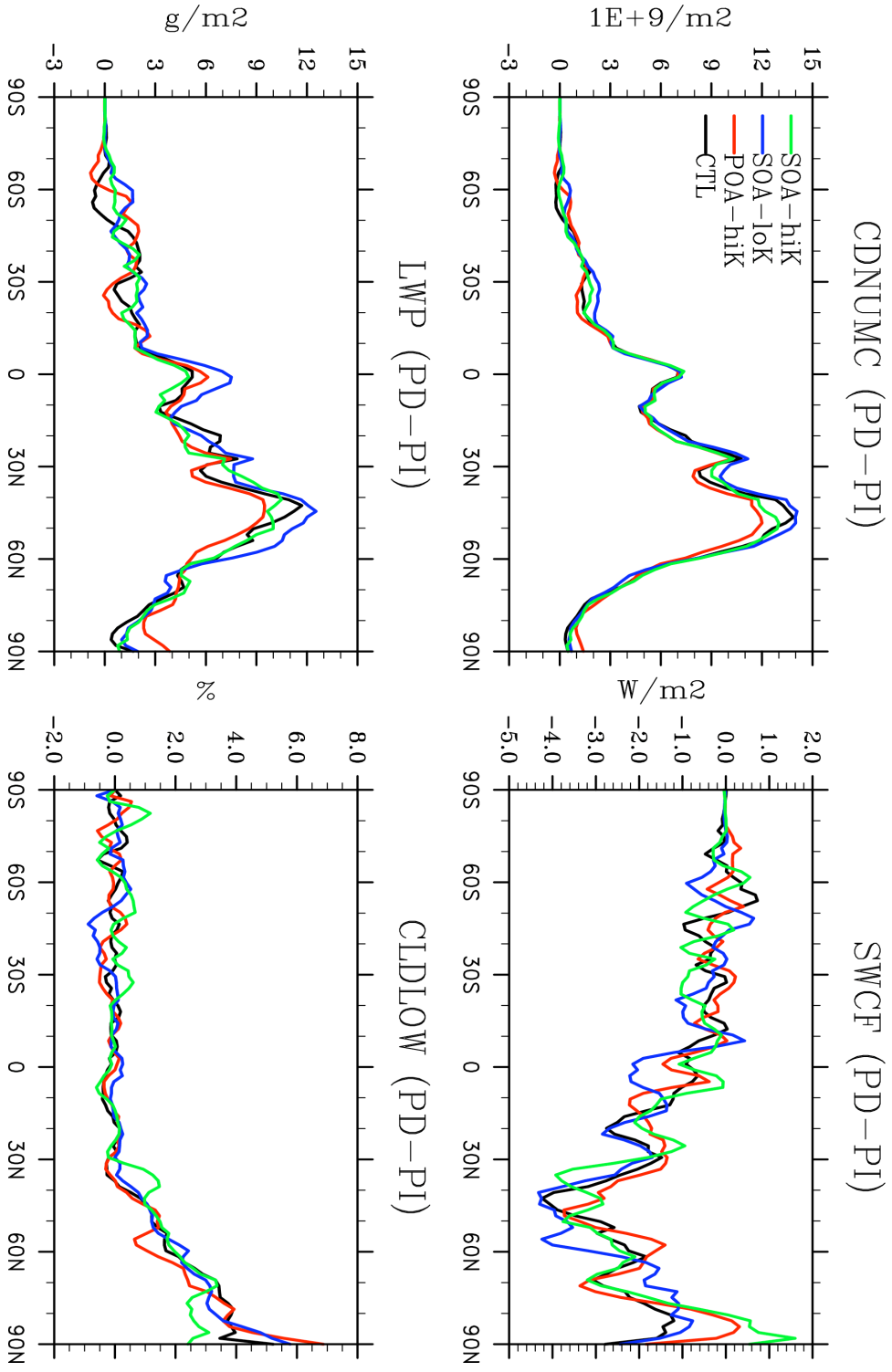

Figure 4. Annual zonal mean changes of column cloud droplet number concentration (CDNUMC), shortwave cloud forcing (SWCF), liquid water path (LWP) and low-level cloud cover (CLDLOW) between PD and PI for the four simulations